

# Error-prone polymerase activity causes multinucleotide mutations in humans

Kelley Harris<sup>1\*</sup> and Rasmus Nielsen<sup>2,3,4</sup>

1 Department of Mathematics, University of California Berkeley, Berkeley, CA, USA

2 Department of Integrative Biology, University of California Berkeley, Berkeley, CA, USA

3 Department of Statistics, University of California Berkeley, Berkeley, CA, USA

4 Center for Bioinformatics, University of Copenhagen, Copenhagen, Denmark

\* E-mail: kharris@math.berkeley.edu

## Abstract

### Abstract

About 2% of human genetic polymorphisms have been hypothesized to arise via multinucleotide mutations (MNMs), complex events that generate SNPs at multiple sites in a single generation [1,2]. MNMs have the potential to accelerate the pace at which single genes evolve and to confound studies of demography and selection that assume all SNPs arise independently. In this paper, we examine clustered mutations that are segregating in a set of 1,092 human genomes, demonstrating that the signature of MNM becomes enriched as large numbers of individuals are sampled. We leverage the size of the dataset to deduce new information about the allelic spectrum of MNMs, estimating the percentage of linked SNP pairs that were generated by simultaneous mutation as a function of the distance between the affected sites and showing that MNMs exhibit a high percentage of transversions relative to transitions. These findings are reproducible in data from multiple sequencing platforms and cannot be attributed to sequencing errors. Among tandem mutations that occur simultaneously at adjacent sites, we find an especially skewed distribution of ancestral and derived dinucleotides, with GC → AA, GA → TT and their reverse complements making up 36% of the total. These same mutations dominate the spectrum of tandem mutations produced by the upregulation of low-fidelity Polymerase ζ in mutator strains of *S. cerevisiae* that have impaired DNA excision repair machinery. This suggests that low-fidelity DNA replication by Pol ζ is at least partly responsible for the MNMs that are segregating in the human population, and that useful information about the biochemistry of MNM can be extracted from the spectrum of linked SNPs in ordinary population genomic data. We incorporate our findings into a mathematical model of the multinucleotide mutation process that can be used to correct phylogenetic and population genetic methods for the presence of MNMs.

## Introduction

One of the core challenges in evolutionary biology is to explain the distribution of mutations in time and space and harness this knowledge to make inferences about the past. When two DNA sequences have numerous differences that are spaced closely together, they are inferred to have been diverging for a relatively long time, the two lineages accumulating mutations at a steady rate since they diverged from their last common ancestor. In contrast, when two sequences have few differences that are spaced far apart, they are inferred to have diverged from a common ancestor relatively recently. This logic is the basis of a widely used class of methods that infer detailed demographic histories from the spacing between SNPs in a sample of whole-genome sequence data [3–6].

To improve the accuracy of population genetic inference from the spacing between SNPs, it will be important to assess the validity of standard assumptions about the mutational process. One such assumption is that mutations occur independently conditional on the genealogical history of the data; however, there are numerous lines of evidence that 1–5% of SNPs in diverse eukaryotic organisms are produced by multinucleotide mutation events (MNMs) that create two or more SNPs simultaneously. If simultaneously generated mutations are regarded as independent during population genetic analysis, the ages of the clustered variants will be overestimated. This could be important not only for the inference of

demographic histories, but also for other endeavors such as the detection of long-term balancing selection. Closely spaced SNPs with ancient times to common ancestry can provide evidence that genetic diversity has been maintained by natural selection [7–9], and simultaneous mutations have the potential to distort or mimic these signals.

One line of evidence for MNM comes from *de novo* mutations that occur in populations of laboratory organisms including *Drosophila melanogaster* [10,11], *Arabidopsis thaliana* [12], *Caenorhabditis elegans* [13,14], and *Saccharomyces cerevisiae* [15], as well as *de novo* mutations detected by looking at human parent-child-trios [1]. Mutations occurring *de novo* are often found clustered together in pairs within distances ranging from 2 bp to tens of kb; such clusters should be exceedingly rare under mutational independence and cannot be explained by mutation hotspots of reasonable intensity [1].

In yeast, there is additional evidence that MNMs are created by the activity of polymerase  $\zeta$ , an error-prone translesion polymerase that extends DNA synthesis past mismatches and damage-induced lesions [16,17]. Pol  $\zeta$  is also responsible for MNMs that occur during somatic hypermutation of DNA that encodes the variable regions of mouse immunoglobulins [18,19]. These results were established by inactivating Pol  $\zeta$  in mutant yeast strains and adult mouse cells. However, it has not been possible to test experimentally whether Pol  $\zeta$  creates heritable MNMs in higher eukaryotes. Pol  $\zeta$  is required for rapid cell proliferation in normal embryonic development, making Pol  $\zeta$  knockout mice embryonically inviable [20–22].

Clusters of *de novo* mutations are not the only line of evidence for heritable MNM in eukaryotes. Additional evidence for MNM has been obtained by looking at patterns of linkage disequilibrium (LD) between older SNPs that segregate in natural populations. Schrider, *et al.* and Terekhanova, *et al.* examined pairs of nearby SNPs in phased human haplotype data and found that the two derived alleles occurred more frequently on the same haplotype than on different haplotypes [1,2]. When two mutations occur independently, their derived alleles should occur on the same haplotype only 50% of the time; in contrast, MNM should always produce mutation pairs with the two derived alleles on the same haplotype. Using a different counting argument, Hodgkinson and Eyre-Walker also concluded that many SNP pairs occurring at adjacent sites were generated by a simultaneous mutational mechanism [23]. They noted that adjacent linked SNPs outnumber SNPs 2 bp apart by a factor of two, when the two types of pairs should have equal frequency under the assumption of independent mutation.

To gather more data about the MNM process, it will be impractical to rely on *de novo* mutations and essential to harness LD information. Although it is easiest to classify a pair of SNPs as a MNM when the mutations are observed *de novo*, eukaryotes have low enough mutation rates that fewer than 1 MNM per genome is expected to occur each generation on average. Motivated by this, we use an LD-based approach to identify signatures of MNM in the 1000 Genomes Phase I data, a public repository of 1,098 phased human genomes [24]. This repository is 100-fold larger than the datasets that were used for previously published studies of MNM, and its size confers a great deal of power to characterize the multinucleotide mutational spectrum. We use coalescent theory to show that a sample of 2,184 haplotypes should contain a much higher ratio of MNMs to single-mutation SNPs in high LD than smaller datasets do, providing increased statistical power to characterize MNMs, and this prediction is corroborated by our analysis of the 1000 Genomes data.

In accordance with earlier studies of MNM, we find that patterns of linkage disequilibrium (LD) between close-together SNPs are incompatible with mutational independence. We show that it instead is well-described by a simple mixture of independent and MNMs. In addition, we are able to leverage the size of the 1000 Genomes dataset to make several novel discoveries about MNMs. First, MNMs are heavily enriched for transversions, with a transition: transversion ratio of about 1:1 in contrast to the 2:1 genomewide average. More importantly, we find that linked mutations in humans are enriched for the same allelic types recorded by Stone, *et al.* in lines of yeast that have nucleotide excision repair (NER) deficiencies and thus rely heavily on Pol  $\zeta$  for translesion synthesis [17]. These frequent MNMs include the dinucleotide mutations  $GA \rightarrow TT$  and  $GC \rightarrow AA$  as well as mutations at non-adjacent sites that

produce homogeneous AA/TT derived allele pairs. Such patterns are unlikely to result from errors in the DNA sequencing process and instead suggest that normal human Pol  $\zeta$  activity generates at least some of the same MNMs that are produced by Pol  $\zeta$  in NER-deficient yeast [17].

## Results

Time-series data is the most direct way to detect simultaneous mutation events, but MNMs can also be inferred from linkage disequilibrium (LD) in data from unrelated individuals. Schrider, *et al.* previously detected simultaneous mutations from LD in a phased diploid genome, observing that SNPs less than 10 bp apart were disproportionately likely to have their derived alleles lie on the same haplotype [1]. In the spirit of this approach, we looked at the prevalence of neighboring SNPs in the 1000 Genomes Phase I data that occur in perfect LD, meaning that the two derived alleles occur in the exact same subset of the 2,184 sequenced haplotypes. We hereafter define a pair of *close LD SNPs* to be a pair occurring less than 100 bp apart in perfect LD.

### Excess nearby SNPs in LD:

We counted 365,238 pairs of close LD SNPs in the 1000 Genomes phase I data with both sites passing strict genotype quality control and having ancestral states that were identifiable from a human/chimp/orang/macaque reference alignment (see Methods). Simultaneous mutations should always create SNPs in perfect LD, and at distances of  $< 100$  bp apart in the human genome, only a small percentage should have their LD disrupted by recombination. However, we also expect independent mutations to create some close LD SNP pairs by chance, and we quantified this expectation by simulating data under a Poisson process model of independent mutation and recombination implemented in `ms` [25]. We simulated a total of  $4.8 \times 10^9$  bp from an alignment of 2,184 haplotypes under a realistic human demographic model [6] and recovered 369,918 close LD SNP pairs. For comparison, we also simulated  $1.8 \times 10^9$  bp of data under the standard neutral coalescent with constant effective population size  $N = 10,000$ , recovering 362,029 close LD SNP pairs.

As shown in Figure 1, the distribution of distances between close LD SNPs were quite different in the simulated and in the real data, with the real data containing about 5-fold more adjacent SNPs in LD and a decaying excess of SNPs separated by up to 20 bp in LD. In contrast, there is comparatively little difference in the distances between SNPs in the data simulated under the realistic and the standard coalescent model, illustrating that the excess of SNPs in close LD cannot be attributed to assumptions regarding the demographic model. Under the coalescent with independent mutation, the abundance of SNP pairs  $L$  bp apart in LD should decline approximately exponentially with  $L$  for small values of  $L$  (see Appendix A), and we find this to hold for the simulated data in Figure 1.

In contrast, the optimal least-squares exponential fit is a poor approximation to the abundance distribution of close LD SNP pairs in the 1000 Genomes data, which we denote by  $N_{LD}(L)$ . A possible explanation is that close linked SNPs are produced by a mixture of two processes, a point-mutation process that is accurately modeled by the coalescent and a MNM process that is not.

### Close linked SNPs have unusual mutation type frequencies:

To our knowledge, no previous work has addressed whether MNMs have the same transition: transversion ratio as ordinary mutations. However, there is abundant evidence that different DNA polymerases produce mutations with different frequencies of ancestral and derived alleles. To investigate this question, we measured the fractions of linked SNP pairs at distance  $L$  that are composed of transitions, transversions, and mixed pairs (one transition plus one transversion). We denote these fractions  $f_{ts}^{LD}(L)$ ,  $f_{tv}^{LD}(L)$ , and  $f_m^{LD}(L)$ . We also measured the analogous fractions  $f_{ts}^{non-LD}(L)$ ,  $f_{tv}^{non-LD}(L)$ , and  $f_m^{non-LD}(L)$  of transitions, transversions, and mixed pairs among SNPs not found in perfect LD.

In human genetic variation data, transitions are approximately twice as common as transversions. If the two mutation types of a SNP pair were chosen independently, we would therefore expect that  $f_{ts} = 0.66^2 = 0.44$ ,  $f_{tv} = 0.33^2 = 0.11$ , and  $f_m = 2 \times 0.66 \times 0.33 = 0.45$ . These predictions are very close

to  $f_{ts}^{\text{non-LD}}(L)$ ,  $f_{tv}^{\text{non-LD}}(L)$ , and  $f_m^{\text{non-LD}}(L)$  for  $L$  between 2 and 100. (Figure 2). For  $L = 1$ ,  $f_{ts}^{\text{non-LD}}(L)$  is larger than expected because of the elevated transition rate at both positions of CpG sites.

Among mutations in perfect LD, we found that  $f_{ts}^{\text{LD}}(L)$ ,  $f_{tv}^{\text{LD}}(L)$ , and  $f_m^{\text{LD}}(L)$  deviate dramatically from the expectation of mutational independence, adding support to the idea that many such SNPs are produced by a nonstandard mutational process. The frequency of transversion pairs declines with  $L$ ; we found that 36.7% of SNP pairs in LD at adjacent sites consisted of two transversions, compared to 11.1% of SNP pairs in LD at a distance of 100 bp and 10.7% of SNP pairs not in LD. These numbers are not just incompatible with a transition: transversion ratio of 2:1, but are also incompatible with two neighboring SNP types being assigned independently. If the SNP types were assigned independently, it should hold that  $\sqrt{f_{ts}(L)} + \sqrt{f_{tv}(L)} = 1$ , an assumption that is violated for small values of  $L$ . We also found excess close LD transversions in human data sequenced by Complete Genomics (see Supplementary Figure S1), suggesting that this pattern is not an artifact of the Illumina sequencing platform or the 1000 Genomes SNP-calling pipeline. Rather, the pattern is consistent with the idea that excess close LD SNPs are generated by a multinucleotide mutational process that has different ancestral and derived allele frequencies from the mutational process that creates single SNPs.

**A parametric description of multinucleotide mutation:**

Figures 1 and 2 suggest that MNMs are required to explain both the sheer abundance of close linked SNPs and their unusual transition: transversion makeup. Motivated by this, we develop a simple parametric method for estimating the relative rates of MNM and linked independent mutation.

As noted previously, the abundance distribution  $N_{\text{LD}}(L)$  of close linked SNP pairs does not follow the exponential distribution that we expect under mutational independence. However, we were able to fit  $N_{\text{LD}}(L)$  to a sum of three exponentials:

$$\widehat{N}_{\text{LD}}(L) = N^{(S1)} \exp(-a^{(S1)}L) + N^{(S2)} \exp(-a^{(S2)}L) + N^{(i)} \exp(-a^{(i)}L) \quad (1)$$

Minimizing the squared-error distance between  $\widehat{N}_{\text{LD}}(L)$  and  $N_{\text{LD}}(L)$ , we were able to estimate the six parameters  $N^{(S1)}$ ,  $a^{(S1)}$ ,  $N^{(S2)}$ ,  $a^{(S2)}$ ,  $N^{(i)}$ ,  $a^{(i)}$  and obtain a good parametric fit to the abundance distribution of close LD SNPs. The first term,  $N_{(S1)}(L) = N^{(S1)} \exp(-a^{(S1)}L)$ , decays over a length scale of about 3 bp, while the second term,  $N_{(S2)}(L) = N^{(S2)} \exp(-a^{(S2)}L)$ , decays over about 50 base pairs. We conjecture that  $N_S(L) = N_{(S1)}(L) + N_{(S2)}(L)$  is a good estimate of the abundance of simultaneous mutations  $L$  bp apart, a claim that we will proceed to test in several ways. Likewise, we conjecture that  $N^{(i)}(L) = N^{(i)} \exp(-a^{(i)}L)$  is a good estimate of the abundance of linked independent mutations. When we measure the abundance distribution  $N_{\text{ms}}(L)$  of close LD SNP pairs in data simulated under a model of independent mutation in Hudson's *ms*, we find it is well described by a single exponential function

$$\widehat{N}_{\text{LD}}^{(\text{ms})}(L) = N^{(\text{ms})} \exp(-a^{(\text{ms})}L) \quad (2)$$

that decays at about the same rate as  $N^{(i)}(L)$ . All numerical parameter estimates are recorded in Table 1.

So far, we have made two novel claims about the MNM process: one is that the abundance of MNMs  $L$ -bp apart is  $N_S(L)$ ; the other is that MNMs have a low transversion to transition ratio. If both of these claims are true, then the decay rate of the ratio  $N_S(L)/N(L)$  should explain the decay rate of  $f_{ts}(L)$  that is recorded in Figure 2. To show that this holds, we start by breaking down the SNP pair distribution  $N_{\text{LD}}(L)$  into the separate abundance distributions of linked transitions, transversions, and mixed SNP pairs:

$$N_{\text{LD}}(L) = N_{\text{LD}}^{\text{ts}}(L) + N_{\text{LD}}^{\text{tv}}(L) + N_{\text{LD}}^{\text{m}}(L) \quad (3)$$

Using these empirical distributions, we estimate a vector of SNP pair type frequencies ( $f_{ts}$ ,  $f_{tv}$ ,  $f_m$ ) for each of the pure exponential functions  $N^{(S1)}(L)$ ,  $N^{(S2)}(L)$ , and  $N^{(i)}(L)$  (see Figure 3). This is

motivated by the idea that independent mutations will have the same transition/transversion breakdown as mutation pairs not found in LD, but that the MNM process may have a different allelic spectrum. For each of the exponential terms  $N_{(S1)}(L)$ ,  $N_{(S2)}(L)$  and  $N_{(i)}(L)$ , we estimate a frequency vector  $(f_{ts}, f_{tv}, f_m)$  subject to the constraint  $f_{ts} + f_{tv} + f_m = 1$  by minimizing the squared-error distances of  $N_{LD}^{ts}(L)$ ,  $N_{LD}^m(L)$ , and  $N_{LD}^{tv}(L)$  from the following respective estimates:

$$\widehat{N}_{LD}^{ts}(L) = f_{ts}^{(S1)} \cdot N^{(S1)}(L) + f_{ts}^{(S2)} \cdot N^{(S2)}(L) + f_{ts}^{(i)} \cdot N^{(i)}(L) \quad (4)$$

$$\widehat{N}_{LD}^m(L) = f_m^{(S1)} \cdot N^{(S1)}(L) + f_m^{(S2)} \cdot N^{(S2)}(L) + f_m^{(i)} \cdot N^{(i)}(L) \quad (5)$$

$$\widehat{N}_{LD}^{tv}(L) = f_{tv}^{(S1)} \cdot N^{(S1)}(L) + f_{tv}^{(S2)} \cdot N^{(S2)}(L) + f_{tv}^{(i)} \cdot N^{(i)}(L) \quad (6)$$

As shown in Figure 3, this model explains how MNMs can explain the change in transition/transversion ratio in close LD SNPs with distance  $(L)$ . In particular, the estimated abundance vector  $(\widehat{N}_{LD}^{ts}(L), \widehat{N}_{LD}^m(L), \widehat{N}_{LD}^{tv}(L))$  is a good approximation to the empirical abundance distribution of close LD SNPs in the 1000 Genomes data. As a consequence of the model, we can estimate the percentage of linked SNP pairs that were produced by simultaneous mutation as a function of the distance  $L$  between the SNPs (see Figure 4). These estimates are uniformly higher for pairs of transversions than for mixed pairs or transitions.

Among SNPs that occur at adjacent sites in perfect LD, we estimate that 85% of transition pairs are caused by MNM and that 98% of transversion pairs are caused by MNM. These percentages are higher than analogous numbers obtained by Schridder, *et al.* and Terekhanova, *et al.* because these authors studied mutations that occurred over longer evolutionary timescales. Terekhanova, *et al.*, for example, estimated that 50% of “lineage-specific substitutions” at adjacent sites were caused by MNM, defining a pair of lineage-specific substitutions to be SNPs where the derived allele appears in a set of 10 human sequences and is absent from a set of outgroup primate sequences. The difference between their estimate and ours can be explained by considering the length  $T$  of the phylogenetic tree branch subtending the sample where the derived alleles occur. If  $\mu$  is the rate of ordinary point mutations per site per generation and  $\mu_{MNM}$  is the analogous rate of MNM at a pair of sites, then assuming  $T$  is known, the probability that two linked mutations were generated simultaneously is  $\mathbb{P}(\text{MNM}|T) = \mu_{MNM}T / (\mu_{MNM}T + \mu^2T^2)$ . As  $T$  approaches zero,  $\mathbb{P}(\text{MNM}|T)$  approaches 1. In the 1000 Genomes data, two linked derived alleles can occur in any subset of 2,184 human haplotypes, meaning that  $T$  may be very short compared to the time it takes for a human clade to coalesce with a nonhuman primate lineage (Figure 5). As a result, adjacent transversions in perfect LD can be identified almost unambiguously as MNMs rather than linked independent mutations.

As the number of sampled lineages goes to infinity, we expect the number of observed MNMs to go to infinity as well, while the number of independent linked mutations should decrease with increasing sample size and approach a finite asymptotic value (see Appendix B). As a result, the percentage of perfect LD SNPs that are MNMs should increase with increasing sample size and the abundance of transversions relative to transitions should increase as well. To test this, we counted perfect LD SNPs in subsets of the 1000 Genomes data containing 2–2,183 haplotypes and calculated the percentages of transition pairs, transversion pairs, and mixed pairs. When the perfect LD SNPs are adjacent, the percentage of transversion pairs increases very quickly with the number of lineages, making up 27% of the total when only 2 haplotypes are sampled and nearly 40% of the total when all 2,184 haplotypes are sampled. For perfect LD SNPs that occur 100–200 bp apart, the percentage of transversion pairs increases much more slowly, but is still 10% higher in a sample of 2,184 haplotypes than in samples of 2 to 1,000 haplotypes (See Figure 6). Because simultaneous mutations 100 bp apart appear to be generated at a very low rate compared to simultaneous mutations at adjacent sites, they only become detectible in samples of hundreds of lineages. This explains why previous work on smaller human datasets was only able to detect MNMs up to 20 bp apart, whereas we infer significant MNM among pairs of linked SNPs at a distance of 50 bp, estimating that 5% of transition pairs and 12% of transversion pairs were created by MNM.

At a distance of 100 bp between linked SNPs, we estimate that only 0.2% of transition pairs and 0.5% of transversion pairs are the result of MNM. However, there is some reason to believe that these figures are underestimates and that MNM creates some SNP pairs that are hundreds of bp apart. The reason is that our estimate of  $(f_{ts}^{(i)}, f_m^{(i)}, f_{tv}^{(i)})$  is slightly different from the frequency distribution  $(f_{ts}^{\text{non-LD}}, f_m^{\text{non-LD}}, f_{tv}^{\text{non-LD}})$  of SNP pairs not in perfect LD, with  $f_{ts}^{(i)} < f_{ts}^{\text{non-LD}}$  and  $f_{tv}^{(i)} > f_{tv}^{\text{non-LD}}$  (as reported in Table 1). It is possible that the linked SNPs we designate as generated by independent mutation have a higher percentage of transversions than unlinked SNP pairs because a small percentage of them were generated by MNMs that are too sparse to be isolated by our model.

**The effect of simultaneous mutation on the site frequency spectrum:**

To obtain further evidence that MNMs are abundant and enriched for transversion pairs, we harness the fact that MNMs and linked independent mutations should have different site frequency spectra (SFS). By a standard Poisson-thinning argument, the SFS does not depend on the rate at which mutations occur; this implies that generic transitions, transversions, and MNMs should all have identical frequency spectra. In contrast, closely positioned independent mutations in perfect LD should be enriched for high frequencies because they depend on repeated mutation at nearby sites with correlated genealogical histories. Such mutations are disproportionately likely to affect long coalescence tree branches; long branches, in turn, are often subtended by many leaves. This is illustrated in Figure 7F, which shows the SFS of both single mutations and mutation pairs in perfect LD in data simulated under a standard coalescent model using independent mutations.

Given a mixture of simultaneous and independent mutations, the SFS should be a linear combination of the site frequency spectra of independent and simultaneous linked mutations. The more heavily the mixture is weighted toward independent mutations, the more the SFS should be skewed toward high frequencies. Based on the results reported so far, we predict that linked SNPs separated by 100–1000 bp should consist almost entirely of independent mutations. In contrast, we predict that 95% of transversions at adjacent sites were produced simultaneously, as well as 70% of transitions at adjacent sites. As expected, we observe that adjacent transversions have the highest frequency of singletons among these classes of sites, while linked SNPs 100–1000 bp apart have the lowest frequency of singletons. Linked SNPs between 2 and 100 bp apart have intermediate frequencies of singletons, with transversion pairs having a the highest frequency of singletons within each distance category. All of these results qualitatively meet our expectation that perfect LD SNP pairs are more prevalent among close-together transversions than among farther-apart transitions (Figure 7).

For comparison, we computed the site frequency spectra of adjacent SNP pairs not in perfect LD. In this case, we found that that transitions, transversions, and mixed pairs all had essentially the same frequency spectra as the population background. In data without MNMs, we found very little difference between site frequencies of SNPs in LD at distances between 1 and 100 bp.

It is likely that some singletons in perfect LD less than 50 bp apart are missing from this dataset because of mapping quality filtering. Most reads that are informative about such SNP pairs will carry at least two differences from the reference genome, giving them lower mapping quality scores than reads with one or zero differences from the reference. However, if mapping quality filtering does skew the SFS toward higher frequencies, it should have the strongest effect on the SNP pairs that are closest together (and thus most often spanned by a single read). This is the opposite of the pattern we actually observe, which is that the frequency of singletons in perfect LD increases with inter-SNP distance.

**Evidence for error-prone synthesis by Polymerase  $\zeta$ :**

One mechanism that generates MNMs *in vivo* is error-prone lesion bypass by Polymerase  $\zeta$ , an enzyme found in all eukaryotes with the unique ability to extend primers with terminal mismatches [26, 27]. At a replication fork that has been stalled by a lesion, Pol  $\zeta$  is responsible for adding bases to the strand containing the lesion and then extending replication for a few base pairs before detaching and allowing a high-fidelity enzyme to resume synthesis. During this extension phase, it has the potential to create clustered errors. Experimental work in yeast has confirmed that Pol  $\zeta$  generates MNMs [16, 17], and the

same enzyme has been linked to somatic hypermutation in the MHC [18, 19].

To look for evidence of Pol  $\zeta$  activity in the human genome, we compared linked adjacent mutations in the 1000 Genomes data to tandem (adjacent) mutations recorded from a yeast strain bred by Stone, *et al.* to be deficient in nucleotide excision-repair machinery and rely heavily on Pol  $\zeta$  to bypass lesions that stall replication forks (see [17]). Stone, *et al.* recorded a total of 61 spontaneous tandem mutations; these were even more heavily weighted toward transversions than linked SNPs in the 1000 Genomes data, with 52.5% transversion pairs, 37.7% mixed pairs, and only 9.8% transition pairs.

Two particular tandem mutations composed more than 60% of the tandem mutations in the Stone, *et al.* yeast. One of them, GA  $\rightarrow$  TT, is a transversion pair that made up 31% of the total. The other, GC  $\rightarrow$  AA, is a mixed pair that made up 30% of the total. We found that these were also by far the most common adjacent linked SNPs in the 1000 Genomes data, with GC  $\rightarrow$  AA comprising 16% of the total and GA  $\rightarrow$  TT comprising 10%. No other single mutation type accounts more than 5% of the linked adjacent mutations in the 1000 Genomes data, and no other type accounts for more than 7% of the Stone, *et al.* tandem mutations (Figure 8).

In addition to 61 tandem mutations affecting adjacent base pairs, Stone, *et al.* recorded 210 complex mutations where two or more substitutions, insertions, and/or deletions occurred at non-adjacent sites within a single 20 bp window. From this dataset, we extracted 84 pairs of simultaneous substitutions at distances of 2–14 bp apart. These pairs had almost the same transition/transversion makeup as the tandem substitutions, being comprised of 53.6% transversions, 36.9% mixed pairs, and 9.5% transitions.

Among the non-adjacent yeast mutation pairs, GA  $\rightarrow$  TT and GC  $\rightarrow$  AA were not particularly common, making up only 4.8% and 1.2% of the total, respectively. However, 44.0% of the derived allele pairs were “AA” or “TT” (compared to 72.1% of adjacent mutation pairs). This percentage is much higher than what we would expect in two mutations that occurred independently. Mutation accumulation studies have shown that 33% of yeast mutations have derived allele A (by A/T symmetry, 33% also have derived allele T) [15]. From this, we expect the fraction of AA/TT derived allele pairs to be only  $2 \times 0.33^2 = 0.22$ .

We found that AA and TT were similarly overrepresented among the derived allele pairs in linked human SNPs. In Figure 9, we plot the fraction  $f_{AA}(L)$  of derived AA/TT allele pairs as a function of the distance  $L$  between perfect LD SNPs, charting its decline from  $f_{AA}(1) = 0.445$  through  $f_{AA}(100) = 0.144$ . As with the transversion abundance function  $f_{tv}(L)$ , we are able to fit  $f_{AA}(L)$  to an estimate

$$\hat{f}_{AA}(L) = f_{AA}^{(S1)} \cdot N^{(S1)}(L) + f_{AA}^{(S2)} \cdot N^{(S2)}(L) + f_{AA}^{(i)} \cdot N^{(i)}(L) \quad (7)$$

that depends on inferred abundances of simultaneous and independent linked mutations, obtaining numerical parameters  $f_{AA}^{(S1)} = 0.497$ ,  $f_{AA}^{(S2)} = 0.223$ , and  $f_{AA}^{(i)} = 0.129$ . Since  $f_{AA}^{(S1)}$  and  $f_{AA}^{(S2)}$  are higher than  $f_{AA}^{(i)}$ , it appears that simultaneous mutations are enriched for derived AA/TT allele pairs in addition to being enriched for transversions, another attribute they share with MNMs caused by Pol  $\zeta$  in yeast lines.

Enough is known about the mechanism of error-prone translesion synthesis to suggest a possible explanation for the three-exponential mixture model that fits the distribution of perfect LD SNPs in the 1000 Genomes data. When a high-fidelity polymerase encounters a DNA lesion and stalls, the stalled fork triggers a ubiquitination signal that recruits an error-prone polymerase for lesion bypass. Once the lesion has been bypassed, another chemical signal is required to recruit a high fidelity polymerase back to the task of replication. Before this occurs, the low-fidelity polymerase usually replicates a stretch of undamaged DNA that is longer than the upstream lesion [27–29]. It is possible that the exponential term  $N^{(S1)}(L)$  decays over a length scale of 2–3 bp because 2–3 bp is the size of a typical DNA lesion created by oxidative damage or ultraviolet light. The second term  $N^{(S2)}(L)$ , which decays over tens of base pairs, could encompass mutations that are introduced downstream of DNA lesions during the time it takes for low-fidelity polymerases to detach and be replaced by high-fidelity ones.

#### **Correcting downstream analyses for multinucleotide mutation:**

As evidenced by Figures 1 and 7, MNMs can have considerable impact on summary statistics like the site frequency spectrum and the prevalence of linkage disequilibrium. These summary statistics provide

clues about the genealogical histories of datasets and can be leveraged to infer demographic history, natural selection, population structure, recombination rates, and other quantities of interest. However, accurate inference depends on accurately modeling the process that generates data, and most population genetic models omit MNMs.

One strategy for improving the accuracy of downstream analyses without adding much to their complexity is to identify MNMs in a probabilistic way and remove them from the data. For each pair of SNPs occurring in perfect LD, we can use our exponential mixture model to estimate the probability that they were caused by a MNM as a function of their inter-SNP distance and transition/transversion status, then use this information to correct summary statistics for the presence of MNMs. To illustrate, we computed the average  $r^2$  correlation coefficient as a function of the distance between SNPs in the 1000 Genomes data and then devised a weighted average  $r_{\text{MNM}}^2$  that corrects for MNMs and estimates the average correlation between independent mutations. As shown in Figure 10,  $r_{\text{MNM}}^2$  is uniformly less than  $r^2$ . Unsurprisingly, the corrected estimate is the most different from the uncorrected estimate for SNPs at adjacent sites, where the percentage of MNMs is highest and  $r_{\text{MNM}}^2$  is only half as large as  $r^2$ .

## Discussion

We have uncovered a strong signature of multinucleotide mutation in 1,092 genomes sequenced by the 1000 Genomes consortium, with a large excess of close LD SNPs that cannot be explained by demography or mutational hotspots. This is consistent with earlier reports of MNM in smaller human datasets; however, MNMs are enriched relative to independent linked SNPs as more lineages are sampled and mutations are localized to increasingly short genealogical branches.

By looking at the allelic composition of close LD SNPs containing MNMs, we found several signatures that are consistent with error-prone lesion bypass by Polymerase  $\zeta$ . One signature is an excess of transversions, the second is an excess of the dinucleotide mutations  $GA \rightarrow TT$  and  $GC \rightarrow AA$ , and the third is a bias toward homogeneous AA/TT derived allele pairs. It remains an open question whether Pol  $\zeta$  is responsible for the majority of human MNMs and how many other DNA damage and repair mechanisms come into play. However, it is interesting that Pol  $\zeta$  appears to create the same mutation types in the human lineage that it creates in yeast with artificial excision repair deficiencies.

An important alternative hypothesis for the observed patterns is DNA sequencing or assembly errors in the 1000 Genomes data, but there are several different lines of evidence that show that our results cannot be explained by such errors. First, we observed similar patterns in data sequenced by Complete Genomics using non-Illumina technology. Secondly, the excess close LD SNPs that are enriched for transversions and AA/TT derived alleles are not only singleton mutations, but occur at a range of higher allele frequencies. Errors could only cause such patterns if they occurred in an identical fashion in multiple individuals, mimicking the frequency distribution expected for mutations. Thirdly, as already noted, the MNMs we infer are enriched for the same types as MNMs that were observed *de novo* in yeast.

Most commonly used methods for analyzing DNA sequences assume that mutations occur independently of each other. The fact that this assumption is violated in human data, and perhaps most other eukaryotic data, may have a strong effect on many methods of inference. Methods based solely on counting mutations, such as SFS based methods [30] will probably be minimally affected and mostly in their measures of statistical confidence. In contrast, methods that explicitly use the spatial distributions of mutations, such as methods based on the distribution of the number of mutations in short fragments of DNA [31–34] should be strongly affected. Several recently developed methods analyze genomic data by explicitly modeling the spatial distribution of independent mutations [3–6], and these are at risk for bias in regions where SNPs are close together. However, confounding of these methods by MNM can be minimized by analyzing only a few individuals at a time and by disregarding pairs of SNPs less than 100 bp apart, which is often coincidentally done for the sake of computational efficiency [4, 6]. MNMs likely have a stronger effect on methods that look at data from many individuals across short, allegedly



non-recombining genomic fragments that are only 1 kb long and contain many SNPs fewer than 100 bp apart [31,34]. However, our results can be used to devise bias-correction strategies, because as illustrated in Figure 4, it is straightforward to estimate the probability that a given pair of linked SNPs is a MNM. This also has the potential to improve the accuracy of phylogenetic tree branch length estimation and molecular-clock-based inferences, as well as dN/dS estimation, and their associated measures of statistical confidence.

Our results are also relevant to the interpretation of evidence that genetic variation is being maintained by balancing selection—such evidence typically involves short loci with closely spaced linked SNPs [7–9]. Incidentally, our results also provide an explanation for the observation of Seplyarskiy, *et al.* that the transition/transversion ratio appears depressed near segregating mutations that are shared among multiple hominids [35] (Supplementary Figure S2).

MNMs have the potential to accelerate evolution by quickly changing several amino acids within a single gene. Our results indicate that they also have the potential to increase both sequence homogeneity and A/T content. There is evidence that repetitive sequences experience more indels and point mutations than sequences of higher complexity [36], possibly due to the recruitment of error-prone polymerases, giving MNM extra potential to speed up local sequence evolution by triggering downstream mutations. We are hopeful that more details about this process can be elucidated by inferring the distribution of MNMs in even larger datasets that confer more information about their allelic spectrum and spatial positioning along the genome. In this way, population sequencing data could provide new information about the biochemistry of replication *in vivo*, providing a way to measure the activity of Pol  $\zeta$  over evolutionary time. Pol  $\zeta$  is tightly regulated in embryonic and adult cells because over- and under-expression can each be harmful; excess error-prone DNA replication increases the genomic mutation rate, but impaired translesion synthesis ability can lead to replication fork stalling, DNA breakage, and translocations that are more harmful than point mutations [27,37–40]. An important avenue for future work will be to assess whether different eukaryotes incur different levels of MNM because of changing evolutionary pressures being exerted on error-prone DNA replication activity throughout the tree of life.

## Methods

**Ascertainment of SNP pairs from the 1000 Genomes Phase I data:** Let an  $L$ -pair denote two SNPs that lie exactly  $L$  base pairs apart in the genome, and let  $N_{LD}(L)$  be the number of  $L$ -pairs in a given dataset that consist of two SNPs in complete linkage disequilibrium. A 1-pair consists of two SNPs that affect adjacent sites in the genome. We obtained  $N_{LD}(L)$  from the 1000 Genomes phase 1 data for  $L$  ranging from 1 to 10000 by counting SNPs where the non-reference allele was present in the same subset of the 2,184 haplotypes and both SNP calls were annotated as passing all strict population genetic quality filters.

We inferred ancestral and derived alleles using the UCSC Genome browser alignments of chimp, orang, and macaque to the hg19 human reference, discarding SNP pairs where we could not infer the ancestral state. Specifically, we retained each  $L$ -pair of SNPs where at least one SNP had the same allele present in at least 3 of the hg19 human reference, the chimp reference, the orang reference, and the macaque reference, annotating that allele and its linked counterpart as the ancestral states and the other alleles as the derived states.

We sampled SNP pairs not in LD by counting all pairs of SNPs that were adjacent in the VCF file where the two non-reference alleles were not present in the same set of haplotypes. A pair separated by 100 bp or less was retained if both sites passed strict population genetic QC (as annotated by mask files downloaded from the 1000 Genomes consortium website) and had a putative ancestral allele shared by at least 3 out of the hg19 human reference, the orang reference, and the macaque reference, annotating that allele and its linked counterpart as the ancestral states and the other alleles as the derived states. In this way, we obtained counts  $N_{\text{non-LD}}(L)$  for  $L$  between 1 and 100.

**Simulating SNP pairs in LD under the coalescent:** The simulated data used to generate Figure (1) was produced using Hudson’s `ms` [25]. We simulated 2,184 human haplotypes (1,092 African and 1,092 European) under the demographic model published in [6] that was previously inferred from tracts of identity by state in the 1000 Genomes trios. Because we were only interested in SNP pairs separated by 100 bp or less, we simulated a total of  $5.6 \times 10^5$  independent “chromosomes” of length 10 kb using the mutation rate  $2.5 \times 10^{-8} \text{ bp}^{-1} \text{ gen}^{-1}$  and the recombination rate  $1.0 \times 10^{-8} \text{ bp}^{-1} \text{ gen}^{-1}$ .

**Fitting an exponential mixture model to the distribution of SNPs in LD:** To obtain the numerical parameter estimates in Table 1, we used the `fmin_bfgs` function from the Python library `scipy.optimize` to minimize the following sum squares function of  $\mathbf{N} = (N^{(S1)}, N^{(S2)}, N^{(i)})$ ,  $\mathbf{a} = (a^{(S1)}, a^{(S2)}, a^{(i)})$ , and  $\mathbf{f} = (f_{ts}^{(S1)}, f_m^{(S1)}, f_{tv}^{(S1)}, f_{ts}^{(S2)}, f_m^{(S2)}, f_{tv}^{(S2)}, f_{ts}^{(i)}, f_m^{(i)}, f_{tv}^{(i)})$ :

$$S(\mathbf{N}, \mathbf{a}, \mathbf{f}) = \sum_{L=1}^{1000} \left( N_{LD}^{ts}(L) - \widehat{N}_{LD}^{ts}(L, \mathbf{N}, \mathbf{a}, \mathbf{f}) \right)^2 + \left( N_{LD}^m(L) - \widehat{N}_{LD}^m(L, \mathbf{N}, \mathbf{a}, \mathbf{f}) \right)^2 + \left( N_{LD}^{tv}(L) - \widehat{N}_{LD}^{tv}(L, \mathbf{N}, \mathbf{a}, \mathbf{f}) \right)^2$$

**Calculating  $r^2$  with a correction for multinucleotide mutation:** Given two SNPs  $s_A, s_B$  with ancestral alleles  $A, B$  and derived alleles  $a, b$ , let  $p_{AB}, p_{Ab}, p_{aB}$ , and  $p_{ab}$  be population frequencies of each of the four associated haplotypes. Let  $p_A, p_a, p_B$ , and  $p_b$  be the allele frequencies at individual loci. One measure of linkage disequilibrium between the loci is the correlation coefficient

$$r^2(s_A, s_B) = \frac{|p_{AB}p_{ab} - p_{aB}p_{Ab}|}{\sqrt{p_A p_a p_B p_b}}.$$

LD decays as a function of the genetic distance between loci. It is often useful to summarize the rate of this decay by computing the average value of  $r^2(s, s')$  over all SNP pairs  $(s, s')$  that occur  $L$  bp apart. Letting  $S(L)$  denote this set of SNP pairs, we define

$$r^2(L) = \frac{1}{|S(L)|} \sum_{(s_1, s_2) \in S(L)} r^2(s_1, s_2).$$

To avoid averaging together the effects of MNM and linked independent mutation, it would be ideal to replace  $S(L)$  with the set of SNP pairs  $L$  bp apart that were produced by independent pairs of mutations.

Although it is not possible to classify a SNP pair in perfect LD as a MNM unambiguously, we can correct for MNM by estimating the probability that each observed SNP  $s$  was generated as part of a pair of simultaneous mutations. This probability,  $\mathbb{P}_{\text{MNM}}(s)$ , is calculated as a function of the nearest SNP  $s_{LD}$  occurring in perfect LD with  $s$ . If  $s$  is not in perfect LD with any other SNP within 1000 bp, we assume that  $s$  was generated by an ordinary point mutation and let  $\mathbb{P}_{\text{MNM}}(s) = 0$ . Otherwise, letting  $A(s, s_{LD})$  denote the allelic state of the pair  $(s, s_{LD})$  (either transitions (ts), transversions (tv), or mixed (m)) and  $L$  denote the distance between  $s$  and  $s_{LD}$ , we estimate that

$$\mathbb{P}_{\text{MNM}}(s) = \frac{f_{A(s, s_{LD})}^{(S1)} \cdot N^{(S1)}(L) + f_{A(s, s_{LD})}^{(S2)} \cdot N^{(S2)}(L)}{f_{A(s, s_{LD})}^{(S1)} \cdot N^{(S1)}(L) + f_{A(s, s_{LD})}^{(S2)} \cdot N^{(S2)}(L) + f_{A(s, s_{LD})}^{(i)} \cdot N^{(i)}(L)} \quad (8)$$

Note that when  $s_1$  and  $s_2$  are in perfect LD and mutually closer to one another than to any other SNP in perfect LD,

$$\frac{1}{2}(\mathbb{P}_{\text{MNM}}(s_1) + \mathbb{P}_{\text{MNM}}(s_2)) = \mathbb{P}_{\text{MNM}}(s_1) = \mathbb{P}_{\text{MNM}}(s_2).$$

After using equation (8) to compute  $\mathbb{P}_{\text{MNM}}(s)$  for each SNP  $s$  that occurs in  $S(L)$ , we use these values to compute a weighted average  $r_{\text{MNM}}^2(L)$  that downweights each SNP by the probability that it is part of a complex mutation pair:

$$r_{\text{MNM}}^2(L) = \frac{\sum_{(s_1, s_2) \in S(L)} r^2(s_1, s_2) (1 - (\mathbb{P}_{\text{MNM}}(s_1) + \mathbb{P}_{\text{MNM}}(s_2))/2)}{\sum_{(s_1, s_2) \in S(L)} 1 - (\mathbb{P}_{\text{MNM}}(s_1) + \mathbb{P}_{\text{MNM}}(s_2))/2}.$$

## Acknowledgments

We thank Jasper Rine for sharing his deep understanding of replication and mutation in eukaryotes. We also thank members of the Nielsen and Slakin laboratories, particularly Josh Schraiber, Mehmet Somel, and Tyler Linderoth, for helpful discussion and comments.

## References

1. Schrider D, Hourmozdi J, Hahn M (2011) Pervasive multinucleotide mutational events in eukaryotes. *Curr Biol* 21: 1051–1054.
2. Terehanova N, Bazykin G, Neverov A, Kondrashov A, Seplyarsky V (2013) Prevalence of multi-nucleotide replacements in evolution of primates and *Drosophila*. *Mol Biol Evol* 30: 1315–1325.
3. Hobolth A, Christensen O, Mailund T, Schierup M (2007) Genomic relationships and speciation times of human, chimpanzee, and gorilla inferred from a coalescent hidden Markov model. *PLoS Genetics* 3: e7.
4. Li H, Durbin R (2011) Inference of human population history from individual whole-genome sequences. *Nature* 475: 493–496.
5. Sheehan S, Harris K, Song Y (2013) Estimating variable effective population sizes from multiple genomes: A sequentially Markov conditional sampling distribution approach. *Genetics* 194: 647–662.
6. Harris K, Nielsen R (2013) Inferring demographic history from a spectrum of shared haplotype lengths. *PLoS Genetics* 9: e1003521.
7. Leffler E, Gao Z, Pfeifer S, Ségurel L, Auton A, et al. (2013) Multiple instances of ancient balancing selection shared between humans and chimpanzees. *Science* 29: 1578–1582.
8. Charlesworth D (2006) Balancing selection and its effects on sequences in nearby genome regions. *PLoS Genetics* 2: e64.
9. Ségurel L, Thompson E, Flutre T, Lovstad J, Venkat A, et al. (2012) The ABO blood group is a trans-species polymorphism in primates. *Proc Natl Acad Sci USA* 109: 18493–18498.
10. Keightley P, Trivedi U, Thomson M, Oliver F, Kumar S, et al. (2009) Analysis of the genome sequences of three *Drosophila melanogaster* spontaneous mutation accumulation lines. *Gen Res* 19: 1195–1201.
11. Schrider D, Houle D, Lynch M, Hahn M (2013) Rates and genomic consequences of spontaneous mutational events in *Drosophila melanogaster*. *Genetics* 194: 937–954.
12. Ossowski S, Schneeberger K, Locas-Liedo J, Warthmann N, Clark R, et al. (2010) The rate and molecular spectrum of spontaneous mutations in *Arabidopsis thaliana*. *Science* 327: 92–94.

13. Denver D, Morris K, Lynch M, Thomas W (2004) High mutation rate and predominance of insertions in the *Caenorhabditis elegans* nuclear genome. *Nature* 430: 679–682.
14. Denver D, Dolan P, Wilhelm L, Sung W, Lucas-Liedo J, et al. (2009) A genome-wide view of *Caenorhabditis elegans* base-substitution mutation processes. *Proc Natl Acad Sci USA* 106: 16310–16314.
15. Lynch M, Sung W, Morris K, Coffey N, Landry C, et al. (2008) A genome-wide view of the spectrum of spontaneous mutations in yeast. *Proc Natl Acad Sci USA* 105: 9272–9277.
16. Sakamoto A, Stone J, Kissling G, McCulloch S, Pavlov Y, et al. (2007) Mutator alleles of yeast DNA polymerase  $\zeta$ . *DNA Repair* 6: 1829–1838.
17. Stone J, Lujan S, Kunkel T (2012) DNA polymerase  $\zeta$  generates clustered mutations during bypass of endogenous DNA lesions in *Saccharomyces cerevisiae*. *Environmental and Molecular Mutagenesis* 53: 777–786.
18. Daly J, Bebenek K, Watt D, Richter K, Jiang C, et al. (2012) Altered Ig hypermutation pattern and frequency in complementary mouse models of DNA polymerase  $\zeta$  activity. *The Journal of Immunology* 188: 5528–5537.
19. Saribasak H, Maul R, Cao Z, Yang W, Schenten D, et al. (2012) DNA polymerase  $\zeta$  generates tandem mutations in immunoglobulin variable regions. *J Exp Med* 209: 1075–1081.
20. Bemark M, Khamlichi A, Davies S, Neuberger M (2000) Disruption of mouse polymerase  $\zeta$  (*rev3*) leads to embryonic lethality and impairs blastocyst development *in vitro*. *Curr Biol* 10: 1213–1216.
21. Esposito G, Godin I, Klein U, Yaspo ML, Cumano A, et al. (2000) Disruption of the *Rev3l*-encoded catalytic subunit of polymerase  $\zeta$  in mice results in early embryonic lethality. *Curr Biol* 10: 1221–1224.
22. Wittschieben J, Shivji M, Lalani E, Jacobs M, Marini F, et al. (2000) Disruption of the developmentally regulated *Rev3l* gene causes embryonic lethality. *Curr Biol* 10: 1217–1220.
23. Hodgkinson A, Eyre-Walker A (2010) Human triallelic sites: evidence for a new mutational mechanism? *Genetics* 184: 233–241.
24. The 1000 Genomes Consortium (2012) An integrated map of genetic variation from 1,092 human genomes. *Nature* 491: 56–65.
25. Hudson R (2002) Generating samples under a Wright-Fisher neutral model of genetic variation. *Bioinformatics* 18: 337–338.
26. Gan G, Wittschieben J, Wittschieben B, Wood R (2008) DNA polymerase zeta (*pol*  $\zeta$ ) in higher eukaryotes. *Cell Res* 18: 174–183.
27. Waters L, Minesinger B, Wiltrout M, D’Sousa S, Woodruff R, et al. (2009) Eukaryotic translesion polymerases and their roles and regulation in DNA damage tolerance. *Microbiol and Mol Biol Rev* 73: 134–154.
28. Chen J, Bozza W, Zhuang Z (2011) Ubiquitination of PCNA and its essential role in eukaryotic translesion synthesis. *Cell Biochem Biophys* 60: 47–60.
29. Lehmann A, Niimi A, Ogi T, Brown S, Sabbioneda S, et al. (2007) Translesion synthesis: Y-family polymerases and the polymerase switch. *DNA Repair* 6: 891–899.

30. Gutenkunst R, Hernandez R, Williamson S, Bustamante C (2009) Inferring the joint demographic history of multiple populations from multidimensional SNP frequency data. *PLoS Genetics* 5: e1000695.
31. Yang Z, Rannala B (1997) Bayesian phylogenetic inference using DNA sequences: a Markov Chain Monte Carlo method. *Mol Biol Evol* 14: 717–724.
32. Wang Y, Hey J (2010) Estimating divergence parameters with small samples from a large number of loci. *Genetics* 184: 363–379.
33. Nielsen R, Wakeley J (2001) Distinguishing migration from isolation: a Markov Chain Monte Carlo approach. *Genetics* 158: 885–896.
34. Gronau I, Hubisz M, Gulko B, Danko C, Siepel A (2011) Bayesian inference of ancient human demography from individual genome sequences. *Nature Genetics* 43: 1031–1034.
35. Seplyarskiy V, Kharchenko P, Kondrashov A, Bazykin G (2012) Heterogeneity of the transition/transversion ratio in *Drosophila* and Hominidae genomes. *Mol Biol Evol* 29: 1943–1955.
36. McDonald M, Wang W, Huang H, Leu J (2011) Clusters of nucleotide substitutions and insertion/deletion mutations are associated with repeat sequences. *PLoS Biology* 9: e1000622.
37. Waters L, Walker G (2006) The critical mutagenic translesion DNA polymerase Rev1 is highly expressed during G<sub>2</sub>/M phase rather than S phase. *Proc Natl Acad Sci USA* 103: 8971–8976.
38. Ogawara D, Muroya T, Yamauchi K, Iwamoto T, Yagi Y, et al. (2010) Near-full-length REV3L appears to be a scarce maternal factor in *Xenopus laevis* eggs that changes qualitatively in early embryonic development. *DNA Repair* 9: 90–95.
39. Northam M, Robinson H, Kochenova O, Scherbakova P (2010) Participation of DNA polymerase  $\zeta$  in replication of undamaged DNA in *Saccharomyces cerevisiae*. *Genetics* 184: 27–42.
40. Lange S, Takata K, Wood R (2011) DNA polymerases and cancer. *Nature Rev Cancer* 11: 96–110.
41. Watterson G (1975) On the number of segregating sites in genetical models without recombination. *Theor Pop Biol* 7: 256–276.

## A Exponential decay of LD over short genomic distances

In data simulated under the standard coalescent with recombination, we saw that the count  $N_{LD}(L)$  of SNPs in perfect LD  $L$  bp apart decays approximately exponentially for  $L$  between 1 and 100 bp. Here, we give a heuristic argument why this should be true in the asymptotic limit  $L \ll 1/\rho$ , where  $\rho$  is the population-scaled recombination rate.

Let  $T_1, \dots, T_L$  be the sequence of  $n$ -leaf coalescence trees that occur at the sites of a sequence of length  $L$  that has been evolving with mutation and recombination parameters  $\theta$  and  $\rho$ . For simplicity, we assume a constant effective population size  $N$ . The rates  $\theta$  and  $\rho$  are population-scaled such that  $\mu = \theta/(4N)$  is the mutation rate per site per generation and  $r = \rho/(4N)$  is the recombination rate per site per generation. Given any of these trees  $T_i$ , let  $P(T_i)$  be the set of points  $(x, y) \in T_i$  with the property that  $x$  and  $y$  lie on the same branch of  $T_i$ . The sequential coalescent yields a natural map from points on  $T_i$  to points on  $T_{i+1}$ , though not every point on  $T_i$  necessarily maps to a point on  $T_{i+1}$  if a recombination has occurred between the sites. Let  $\epsilon_{x,y}(T_i)$  be defined such that  $1 - \epsilon_{x,y}(T_i)$  is the probability that  $x$  and  $y$  both map to  $T_{i+1}$ ,  $(x, y) \in P(T_{i+1})$ , and the branch containing  $(x, y)$  subtends the same set of lineages in both  $T_i$  and  $T_{i+1}$ .

A pair of points  $(x, y) \in P(T_i)$  can give rise to a pair of SNPs in perfect LD at sites  $i$  and  $j$  if the following events occur: E1) a mutation occurs at position  $x$  on tree  $T_i$ , E2)  $x$  and  $y$  map to a single branch of each tree between  $T_i$  and  $T_j$  that subtends the same set of lineages, and E3) A mutation occurs at position  $y$  on tree  $T_j$ . Not every pair of SNPs in perfect LD must correspond to a pair of points  $x, y$  satisfying E1–E3; for example, the integrity of the clade by the branch containing  $x$  and  $y$  could be broken up and re-formed by two separate recombinations occurring between sites  $i$  and  $j$ . If the sample size  $n$  is relatively large, however, it will be combinatorially unlikely for any clade to re-form after it has been broken up by recombination, particularly within a very short genomic window. Motivated by this, we will estimate  $N_{\text{LD}}(L)$  assuming that all linked SNP pairs arise at pairs of points  $(x, y)$  that satisfy E1–E3 for some  $T_i$  and  $T_j$ .

Integrating over  $x, y$  and  $T_i, \dots, T_{i+L}$ , we compute that the probability of observing a pair of SNPs in perfect LD at sites  $i$  and  $i + L$  is the following:

$$\begin{aligned} N_{\text{LD}}(i, i + L) &= \theta^2 \int_{T_i, \dots, T_{i+L}} \int_{(x, y) \in P(T_i)} (1 - \epsilon_{x, y}(T_i)) \cdots (1 - \epsilon_{x, y}(T_{i+L})) d_{(x, y)} d_{(T_i, \dots, T_{i+L})} \\ &= \theta^2 + \theta^2 \sum_{k=1}^L (-1)^k \int_{T_i, \dots, T_{i+L}} \int_{(x, y) \in P(T_i)} \sum_{i \leq j_1 < \dots < j_k \leq i+L} \epsilon_{x, y}(T_{j_1}) \cdots \epsilon_{x, y}(T_{j_k}) d_{(x, y)} d_{(T_i, \dots, T_{i+L})}. \end{aligned} \quad (9)$$

Let  $\ell(T)$  denote the total branch length of tree  $T$ . Since any alteration of tree structure requires a recombination event,  $\epsilon_{x, y}(T) \leq \rho \cdot \ell(T)$ . This implies that

$$\sum_{i \leq j_1 < \dots < j_k \leq i+L} \epsilon_{x, y}(T_{j_1}) \cdots \epsilon_{x, y}(T_{j_k}) \leq (\epsilon_{x, y}(T_i) + \dots + \epsilon_{x, y}(T_{i+L}))^k \leq (L\rho(\ell(T_i) + \dots + \ell(T_{i+L})))^k \quad (10)$$

for every  $k$ . Letting  $T^{(2)}$  denote the sum of squares of the branch lengths of a coalescent tree  $T$ , this implies that

$$\begin{aligned} N_{\text{LD}}(i, i + L) &= \theta^2 - \theta^2 \int_{T_i, \dots, T_{i+L}} \int_{(x, y) \in P(T_i)} \rho(\epsilon_{x, y}(T_i) + \dots + \epsilon_{x, y}(T_{i+L})) d_{(x, y)} d_{(T_i, \dots, T_{i+L})} + O((\rho L)^2) \\ &= \theta^2 \mathbb{E}(T^{(2)}) (1 - \rho L \cdot \mathbb{E}(\epsilon_{x, y}(T_i))) + O((\rho L)^2) \end{aligned} \quad (11)$$

$$= \theta^2 \mathbb{E}(T^{(2)}) \exp(-\rho L \cdot \mathbb{E}(\epsilon_{x, y}(T_i))) + O((\rho L)^2) \quad (12)$$

In human-like data where  $N = 10,000$  and  $\rho = 0.0004$ , we can see that  $\rho L \leq 0.04 \ll 1$  when  $L < 100$ , putting us in the appropriate asymptotic realm for perfect LD to decay exponentially with distance.

## B Enrichment of MNMs in large datasets

As a consequence of the argument in Appendix A, we saw that the abundance of linked independent mutations in a sample of  $n$  lineages is proportional to the expected sum of squared branch lengths in an  $n$ -leaf coalescence tree. This is a simple consequence of the fact that two mutations must affect a single branch to create SNPs in perfect LD. In contrast, the abundance of MNMs should be proportional to the total tree length, just as the total number of segregating sites is proportional to the expected tree length.

It is a standard result in population genetics that the expected total tree length  $\mathbb{E}(T_{\text{total}})$  equals the harmonic number  $\sum_{i=1}^{n-1} 1/i$  [41]. To show this, let  $T_i$  be the length of time that the a random genealogy has exactly  $i$  lineages, which has distribution function  $f_i(t) = \binom{i}{2} \exp(-t \binom{i}{2})$ . It follows that

$$\mathbb{E}(T_{\text{total}}) = \mathbb{E} \left( \sum_{i=2}^n i T_i \right) = \sum_{i=2}^n i \mathbb{E}(T_i) = \sum_{i=2}^n i \cdot \frac{2}{i(i-1)} = \sum_{i=1}^{n-1} \frac{1}{i} \approx \log(n-1) \quad (13)$$

Therefore, if  $\mu_{\text{MNM}}$  is the rate of MNMs per coalescent time unit, the expected number of MNMs approaches infinity with increasing  $n$  at the asymptotic rate  $\mu_{\text{MNM}} \log(n)$ .

In contrast, if  $\mu$  is the rate of ordinary point mutations, linked independent mutations appear at the rate  $\mu^2 \mathbb{E}(T_{\text{total}}^{(2)})$ , where  $T_{\text{total}}^{(2)}$  is the sum of squares of the coalescent tree branch lengths. We can show that  $\mathbb{E}(T_{\text{total}}^{(2)})$  approaches a constant as  $n \rightarrow \infty$ . To proceed, we let  $\ell_1, \dots, \ell_n$  denote the lengths of the  $n$  leaves of the tree and  $b_{n-1}, \dots, b_2$  denote the lengths of the  $n - 2$  internal branches, indexed such that the more recent endpoint of branch  $i$  is the first time when the tree has  $i$  lineages:

$$\mathbb{E}(T_{\text{total}}^{(2)}) = n\mathbb{E}(\ell_n^2) + \sum_{i=2}^{n-1} \mathbb{E}(b_i^2). \quad (14)$$

Given that a branch is present when the tree has  $i$  lineages, the probability that the branch is ended by the next coalescence event is  $(i-1)/\binom{i}{2} = 2/i$ . Therefore, given  $j < i$ , the probability that  $b_i = T_i + \dots + T_j$  is

$$\mathbb{P}(b_i = T_i + \dots + T_j) = \left(1 - \frac{2}{i}\right) \cdots \left(1 - \frac{2}{j+1}\right) \cdot \frac{2}{j} = \frac{(i-2) \cdots (j-1) \cdot 2}{i \cdots (j+1) \cdot j} = \frac{2(j-1)}{i(i-1)}. \quad (15)$$

It follows that

$$\mathbb{E}(b_i^2) = \sum_{j=2}^i \mathbb{P}(b_i = T_i + \dots + T_j) \cdot \mathbb{E}((T_i + \dots + T_j)^2) \quad (16)$$

$$= \sum_{j=2}^i \frac{2(j-1)}{i(i-1)} \left( \sum_{k=j}^i \mathbb{E}(T_k^2) + 2 \sum_{j \leq k < \ell \leq i} \mathbb{E}(T_k) \mathbb{E}(T_\ell) \right) \quad (17)$$

$$= \sum_{j=2}^i \frac{2(j-1)}{i(i-1)} \left( \sum_{k=j}^i \frac{8}{k^2(k-1)^2} + \sum_{j \leq k < \ell \leq i} \frac{8}{k(k-1)\ell(\ell-1)} \right) \quad (18)$$

$$= \sum_{j=2}^i \frac{2(j-1)}{i(i-1)} \left( \sum_{k=j}^i \frac{4}{k^2(k-1)^2} + \left( \sum_{k=j}^i \frac{2}{k(k-1)} \right)^2 \right). \quad (19)$$

$$= \sum_{j=2}^i \frac{2(j-1)}{i(i-1)} \left( \frac{4}{3} \left( \frac{1}{j^3} - \frac{1}{i^3} \right) + \left( \frac{2}{j-1} - \frac{2}{i} \right)^2 + O\left( \frac{1}{j^4} + \frac{1}{i^4} \right) \right). \quad (20)$$

$$= \frac{2}{i(i-1)} (4 \log(i-1) - 3/2) + O(i^{-3}). \quad (21)$$

This implies that

$$\mathbb{E}(T_{\text{total}}^{(2)}) = n\mathbb{E}(b_n^2) + \sum_{i=2}^{n-1} \mathbb{E}(b_i^2) \quad (22)$$

$$= \frac{8 \log(n-1)}{n-1} + \sum_{i=2}^{n-1} \frac{8 \log(i-1)}{i(i-1)} + O(1/n) \quad (23)$$

$$= \frac{1}{2}(\log(2) + 1) + \frac{7 \log(n-1)}{n-1} + O(1/n), \quad (24)$$

which decreases asymptotically to the limit  $(\log(2) + 1)/2$  as  $n$  approaches infinity.

It may seem counterintuitive that  $\mathbb{E}(T_{\text{total}}^{(2)})$  decreases as more lineages are sampled and  $\mathbb{E}(T_{\text{total}})$  increases unboundedly, but in both simulated and real data we observe fewer SNPs in perfect LD in a

sample of 2,184 haplotypes than in a subset of e.g. 1,000 haplotypes. To explain why, we note that the total tree length grows at rate  $\log(n)$  as more lineages are sampled, but the tree length is subdivided among distinct branches at the faster rate  $O(1/n)$ . Because branch subdivision occurs faster than the growth rate of the total tree length, the sum of squared branch lengths decreases with increasing sample size, reducing the prevalence of independent linked SNPs and enhancing the signature of MNMs.

## Figure Legends

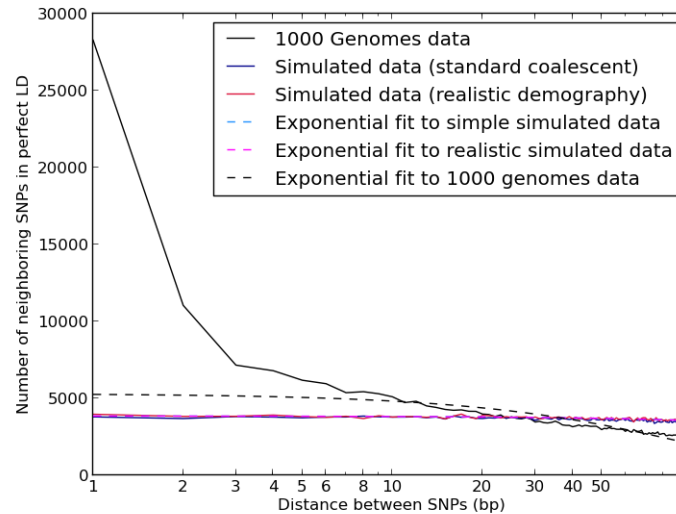


**Figure 1. Nearby SNPs in LD: 1000 Genomes Phase I data vs. simulation under mutational independence.** When we simulated 2,184 haplotypes under a realistic demographic model, we observed 369,918 SNP pairs in LD separated by less than 100 bp in a sample of total length  $4.8 \times 10^9$  bp. Among these pairs, the spacing between SNPs was distributed almost uniformly, with 3,967 at a distance of 1 bp as opposed to 3,544 separated by 99 bp. We observed much less uniformity in the distribution of distances between SNP pairs in LD in the 1000 Genomes data, with an extreme excess of SNPs in LD at 1–2 bp and a less extreme excess of SNPs at distances up to 20 bp apart.

## Tables



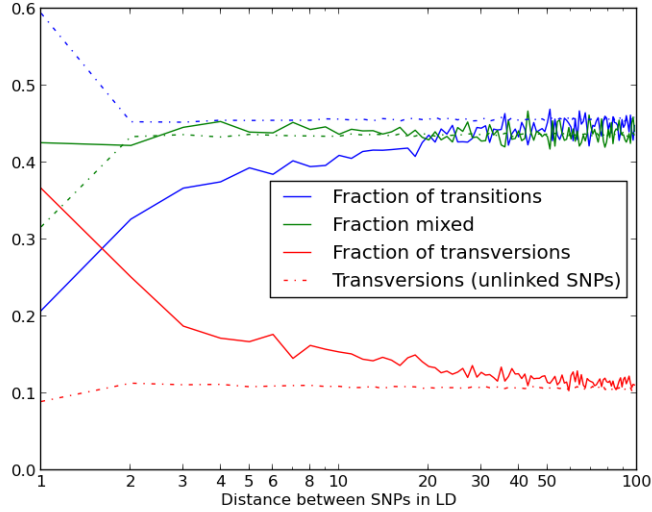


**Figure 2. The relationship between LD and the transition:transversion ratio.** In this figure, the solid blue line plots the fraction of SNP pairs in LD that consist of 2 transitions. The fraction increases quickly as a function of the distance  $L$  between SNPs, asymptotically approaching the fraction of SNP pairs not in LD that consist of 2 transitions. The fraction of SNP pairs not in LD that consist of 2 transitions is nearly constant as a function of  $L$  except for an excess of adjacent transition pairs resulting from double mutation at CpG sites. Although transversion pairs make up just over 10% of unlinked SNP pairs, they account for nearly 40% of adjacent SNPs in perfect LD and about 15% of SNPs in LD at a distance of 10 bp apart.

**Table 1. Parameters estimated from  $N_{LD}(L)$**

$N^{(S1)}$	$a^{(S1)}$	$N^{(S2)}$	$a^{(S2)}$	$N^{(i)}$	$a^{(i)}$	$N^{(ms)}$	$a^{(ms)}$
$1.06 \times 10^5$	1.68	$2.76 \times 10^3$	0.0663	$1.57 \times 10^3$	$5.25 \times 10^{-4}$	$3.85 \times 10^{-3}$	$8.10 \times 10^{-4}$
$f_{ts}^{(S1)}$	$f_{ts}^{(S2)}$	$f_{ts}^{(i)}$	$f_{ts}^{(non-LD)}$	$f_m^{(S1)}$	$f_m^{(S2)}$	$f_m^{(i)}$	$f_m^{(non-LD)}$
0.1524	0.3231	0.4390	0.4576	0.4175	0.4319	0.4426	0.4354
$f_{tv}^{(S1)}$	$f_{tv}^{(S2)}$	$f_{tv}^{(i)}$	$f_{tv}^{(non-LD)}$				
0.4301	0.2450	0.1184	0.1070				

These parameter estimates were generated by fitting equation (1) to the abundance distribution  $N_{LD}(L)$  of linked SNPs  $L$  bp apart in the 1000 Genomes data.  $N^{(S1)}$ ,  $N^{(S2)}$ , and  $N^{(i)}$  are the estimated numbers of close simultaneous mutations, simultaneous mutations and independent mutations in LD at adjacent sites. The decay parameters  $a^{(S1)}$ ,  $a^{(S2)}$ , and  $a^{(i)}$  are defined such that  $N^{(S1)} \exp(-L \cdot a^{(S1)})$ ,  $N^{(S2)} \exp(-L \cdot a^{(S2)})$ , and  $N^{(i)} \exp(-L \cdot a^{(i)})$  are the estimated abundances of linked SNPs  $L$  bp apart in each category. For comparison, the exponential function  $N^{(ms)} \exp(-L \cdot a^{(ms)})$  was fit to data simulated by Hudson's *ms* under a realistic demographic scenario (see Methods).

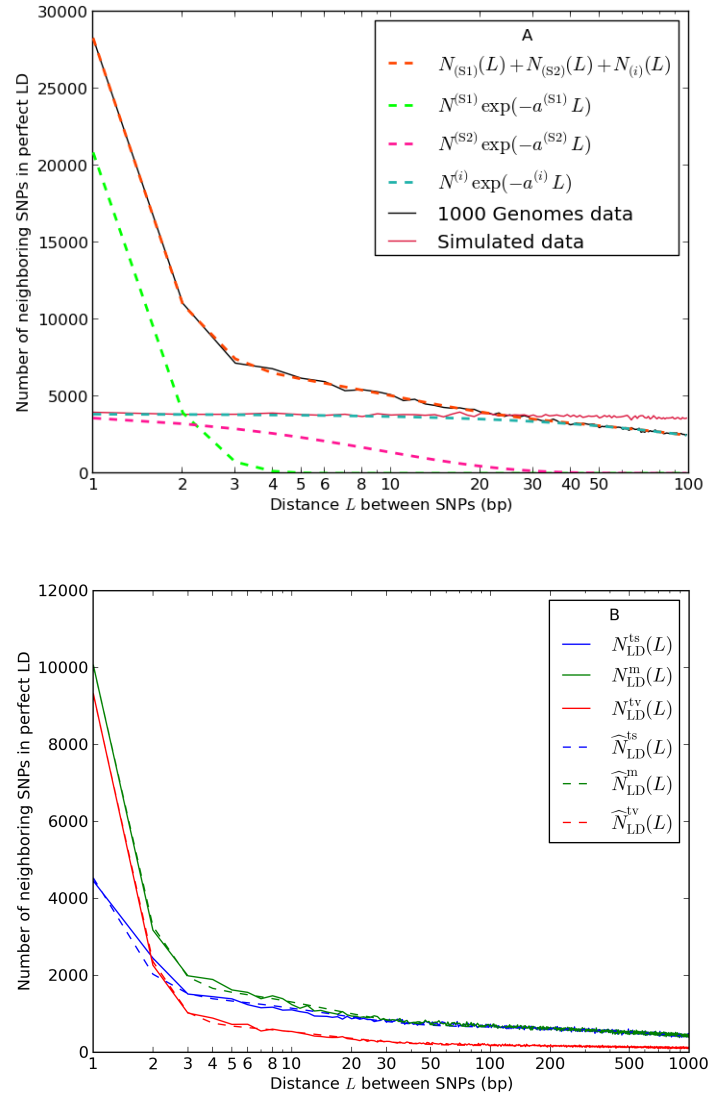


**Figure 3. Decomposition of linked SNP pairs into MNMs and nonsimultaneous mutations.**

The black solid line plotting the abundance of linked SNPs as a function of the distance between them is well-fit by the sum of three exponentials shown in orange. The three exponential summands are shown separately in green, pink, and blue. Using the transition/transversion abundance data in the right-hand plot, we inferred a frequency distribution ( $f_{ts}$ ,  $f_m$ ,  $f_{tv}$ ) for each of the three exponential components. Based on its transition/transversion composition and its similarity to the abundance of linked SNPs in simulated data, we infer that the blue curve is the contribution of independent mutations while the other two are MNMs.

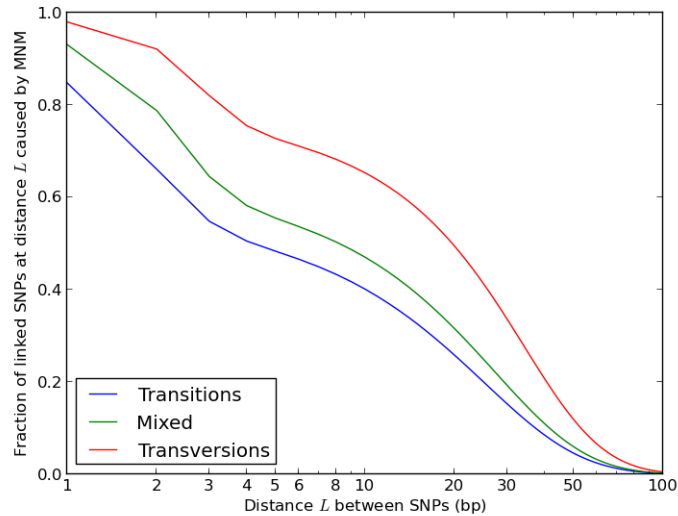


**Figure 4. The fraction of SNPs in perfect LD caused by MNM.** The red curve plots our estimate of the fraction of SNPs in perfect LD at distance  $L$  that were caused by simultaneous mutation. It is uniformly higher than our corresponding estimates for mixed pairs and transitions, plotted in green and blue.

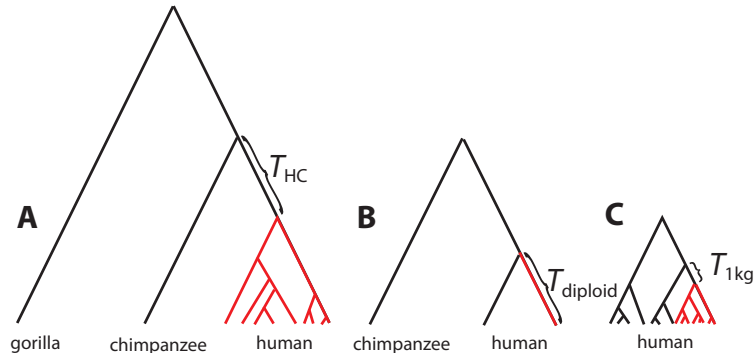


**Figure 5. Three sampling schemes for the detection of MNMs.** Each of these three coalescent trees includes a red clade subtended by a labeled ancestral branch. The length  $T$  of the ancestral branch determines the number of mutations and MNMs that we will observe to be private to the red clade. If  $\mu_{\text{MNM}}(L)$  is the rate of simultaneous mutations separated by  $L$  bp and  $\mu$  is the rate of ordinary point mutations, then the fraction of linked pairs at distance  $L$  that were caused by MNM is expected to be  $\mathbb{P}(\text{MNM}|T) = \mu_{\text{MNM}}T / (\mu_{\text{MNM}}T + \mu^2T^2)$ , which approaches 1 as  $T$  approaches 0. Figure A represents the sampling scheme used by Terekhanova, *et al.* [2], who looked for multinucleotide substitutions on the human lineage after divergence from chimp. Figure B represents a different scheme used by Schrider, *et al.* [1], who looked for more recent MNMs on one lineage of a phased diploid human genome. Figure C represents the sampling scheme we use in this paper, where putative MNMs occur on very short internal branches of a genealogy of 2,184 human haplotypes. Since  $T_{1\text{kg}}$  is typically much smaller than  $T_{\text{diploid}}$  or  $T_{\text{HC}}$ , we observe a higher ratio of MNMs to other SNP pairs in perfect LD.

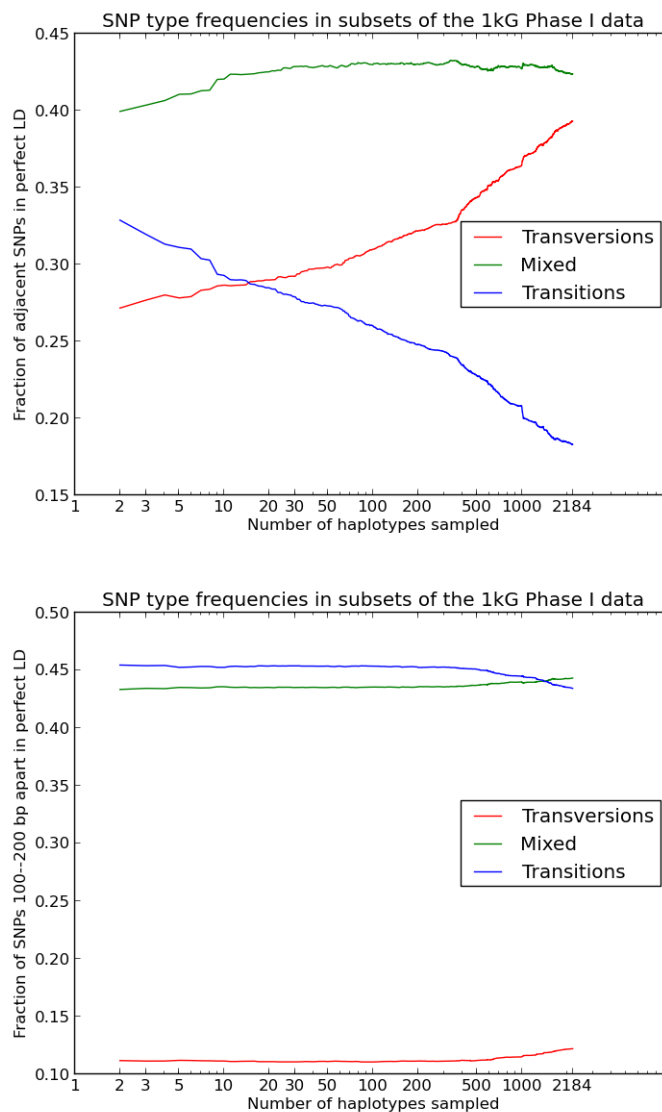


**Figure 6. Enrichment of transversion pairs and MNMs with increasing sample size.** We generated subsamples of the 1000 Genomes data containing 2–2,184 haplotypes and computed the percentages of transversion pairs, transition pairs, and mixed pairs for perfect LD SNPs in each dataset. When the perfect LD SNPs are adjacent, the percentage of transversion pairs nearly doubles as the sample size increases from 2 to 2,184 haplotypes. This percentage increases slowly but detectably among perfect LD SNPs that lie 100–200 bp apart, indicating that MNMs are much less common at this distance but are still evident in large samples.

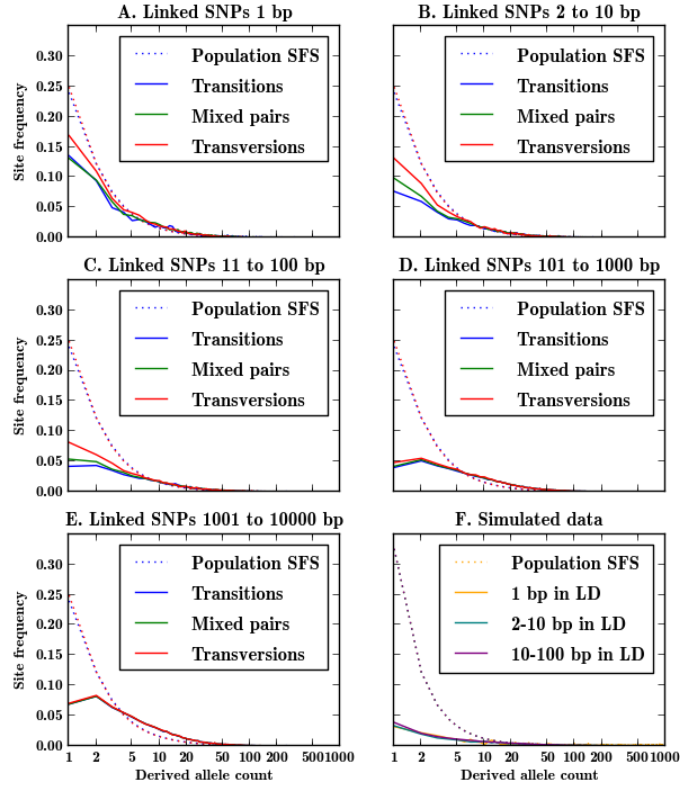


**Figure 7. Site frequency spectra of mutations in perfect LD.** Each of the first five panels contains site frequency spectra of transitions, mixed pairs, and transversions found in perfect LD in the 1000 Genomes data. The pairs are categorized by the order of magnitude of the distance between the SNPs. For comparison, the population-wide frequency spectra of transitions and transversions are plotted as dotted lines. As expected, these two spectra are identical; however, linked SNP pairs have a higher frequency of singletons when they contain one or two transversions. We attribute this effect to a higher proportion of MNMs among transversion pairs and mixed pairs. In the bottom right hand panel, we plot the site frequency spectra of linked SNPs in simulated data. The simulated frequency spectra vary little with inter-SNP distance.

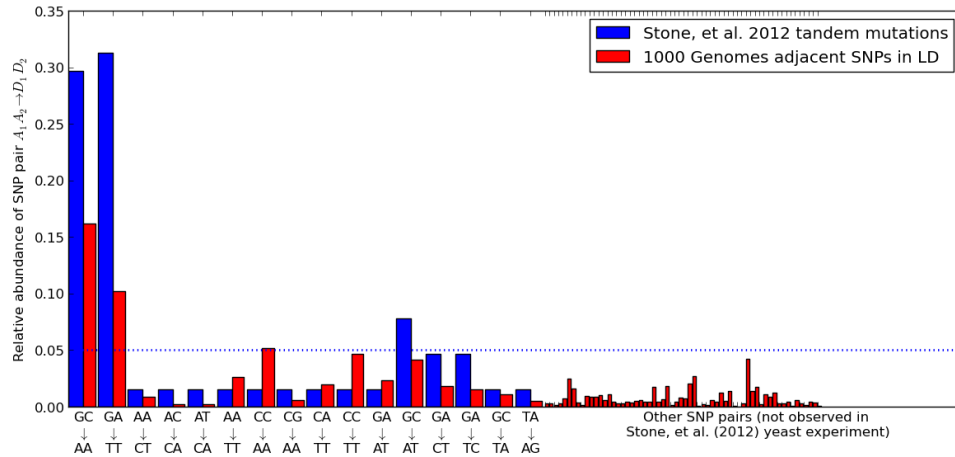


**Figure 8. Tandem mutations caused by Pol  $\zeta$ .** Blue bars plot the frequencies of specific tandem mutations observed by Stone, *et al.* in yeast deficient in nucleotide-excision repair machinery. Each mutation type is pooled with its reverse complement because there is no way to know on which DNA strand a mutation occurred. The two mutations GC  $\rightarrow$  AA and GA  $\rightarrow$  TT account for more than 60% of all tandem mutations observed by Stone, *et al.* As shown in red, these are also the two most common types of mutations occurring at adjacent sites of the 1000 Genomes data in perfect LD.

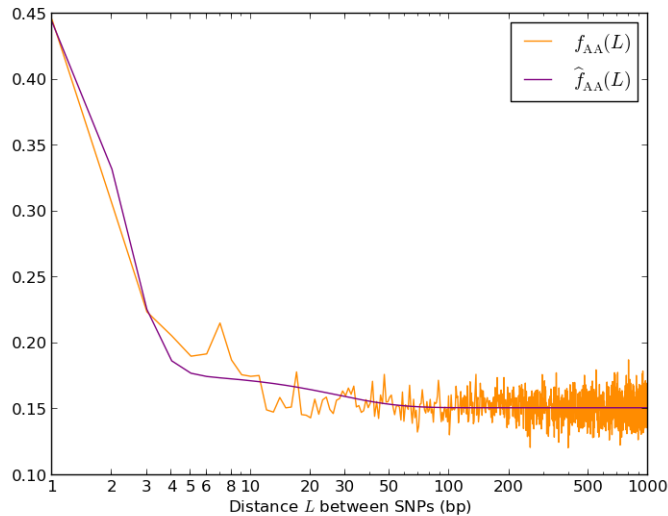


**Figure 9. Linked derived AA/TT allele pairs in the 1000 Genomes data.** After observing that a high fraction of yeast MNMs had homogeneous AA/TT derived allele pairs, we tabulated the frequencies  $f_{AA}(L)$  of AA/TT derived allele pairs among linked SNPs  $L$  bp apart in the 1000 Genomes data. Here,  $f_{AA}(L)$  is plotted alongside the theoretical estimate  $\hat{f}_{AA}(L)$  from equation (7), which posits that MNMs produce AA/TT derived allele pairs 2–4 times as often as independent mutation pairs do.

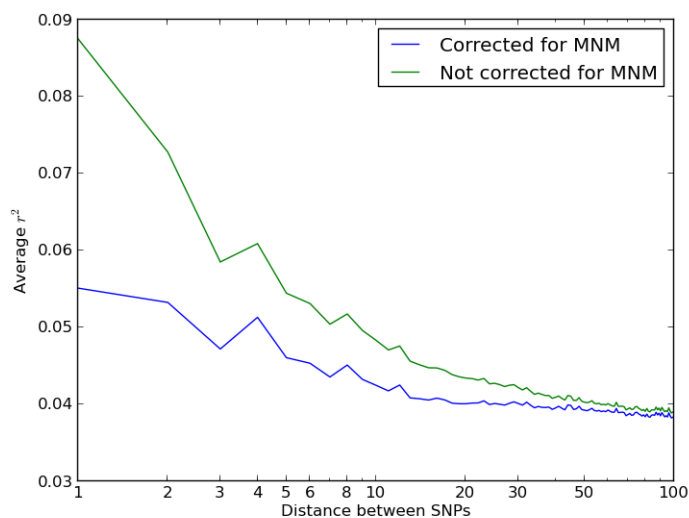
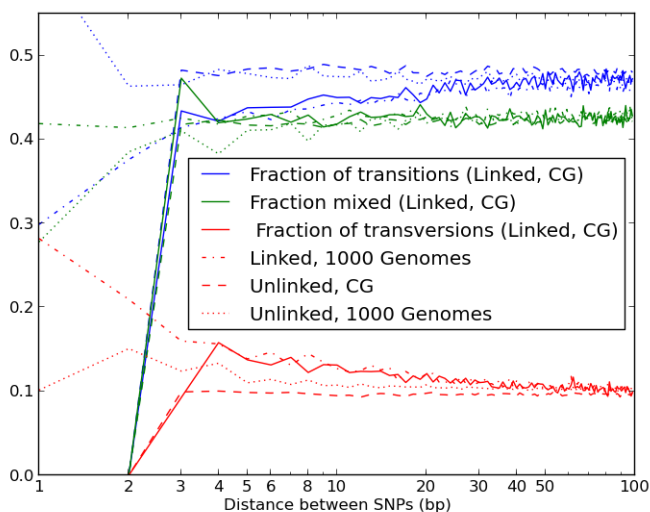
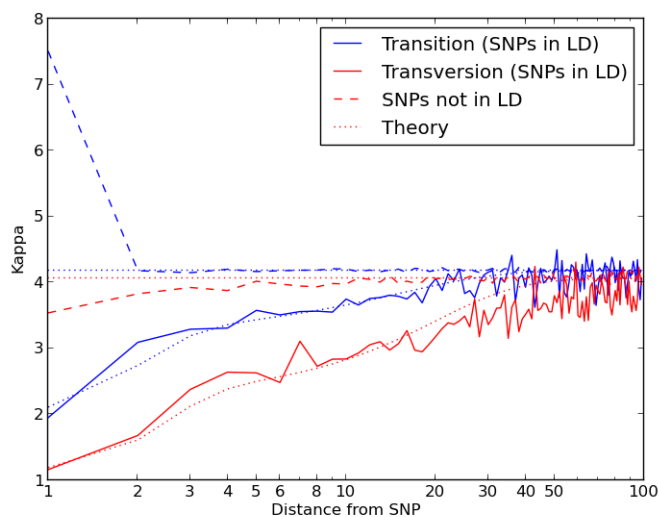


**Figure 10. Average  $r^2$  LD correlations between 1000 Genomes SNP pairs.** The correlation coefficient  $r^2$  between allele frequencies at neighboring sites is often used to measure the decay rate of genealogical correlation with genomic distance. However, we have seen that multinucleotide mutation creates excess LD compared to the expectation under independent mutation. We computed the average  $r^2$  across all SNP pairs  $L$  bp apart on chromosome 22, then corrected this value for the presence of MNM.



**Supplementary Figure S1. Consistency of the transition: transversion ratio across linked SNPs from different sequencing platforms.** To make this figure, we classified pairs of nearby SNPs in 54 unrelated humans sequenced by Complete Genomics. For comparison, we subsampled 54 genomes from the 1000 Genomes Phase I dataset that had approximately the same population breakdown as the Complete Genomics dataset. For each dataset, we counted all SNP pairs occurring less than 100 bp apart, recording whether they occurred in perfect LD and whether they consisted of transitions, transversions or a mixture of the two. Because of stringent filtering against adjacent and nearby SNPs, human data sequenced by Complete Genomics contains no SNPs closer than 3 bp apart. However, close linked SNPs between 3 and 100 bp apart show a depressed transition: transversion ratio that decays with distance at the same rate that it decays in the 1000 Genomes data (see Figure 2). In each dataset, there is little to no dependence at non-CpG sites on the base composition of SNPs not in LD and the distance between the SNPs.





**Supplementary Figure S2. Explaining the variation of  $\kappa$  in the neighborhood of a SNP.** It is common to summarize the transition: transversion ratio with a parameter  $\kappa$  for which  $f_{\text{transversion}} = 2/(\kappa + 2)$ . On average,  $\kappa = 4$  in the human genome, meaning that each type of transition is 4 times as abundant as a particular type of transversion. Looking only at SNPs in LD,  $\kappa$  appears significantly depressed in the neighborhood of a segregating SNP, suggesting that a negative positional correlation between mutation rate and  $\kappa$ . However, this effect is not apparent among SNPs that are not in LD.  $\kappa$  is elevated, on average, at the site next to a transition because of adjacent transitions generated by mutations at both positions of a CpG site. In addition,  $\kappa$  appears slightly reduced among unlinked SNPs in the neighborhood of a transversion, suggesting that there is some regional variation in  $\kappa$  but not as much as appears to be the case if simultaneous mutations are regarded as independent.